

# EMind: A Foundation Model for Multi-task Electromagnetic Signals Understanding

Luqing Luo<sup>1†</sup>, Wenjin Gui<sup>4†</sup>, Yunfei Liu<sup>3</sup>, Ziyue Zhuang<sup>4</sup>, Yunxi Zhang<sup>4</sup>,  
Fengxiang Wang<sup>5</sup>, Zonghao Guo<sup>2</sup>, Qirui Zhao<sup>7</sup>, Zizhi Ma<sup>6</sup>, Xinzhu Liu<sup>3</sup>, Hanxiang He<sup>4</sup>,  
Jinhai Li<sup>1</sup>, Xin Qiu<sup>1</sup>, Wupeng Xie<sup>3\*</sup>, Yangang Sun<sup>2\*</sup>

<sup>1</sup>Institute of Microelectronics of the Chinese Academy of Sciences, China; <sup>2</sup>Tsinghua University, China

<sup>3</sup>Artificial Intelligence Institute of China Electronics Technology Group Corporation, China

<sup>4</sup>Beijing Institute of Technology, China; <sup>5</sup>National University of Defense Technology, China

<sup>6</sup>Nankai University, China; <sup>7</sup>Northeastern University, China

<sup>†</sup>These authors contributed equally to this work.

**Abstract**—Deep understanding of electromagnetic signals is fundamental to dynamic spectrum management, intelligent transportation, autonomous driving and unmanned vehicle perception. The field faces challenges because electromagnetic signals differ greatly from text and images, showing high heterogeneity, strong background noise and complex joint time frequency structure, which prevents existing general models from direct use. Electromagnetic communication and sensing tasks are diverse, current methods lack cross task generalization and transfer efficiency, and the scarcity of large high quality datasets blocks the creation of a truly general multitask learning framework. To overcome these issue, we introduce EMind, an electromagnetic signals foundation model that bridges large scale pretraining and the unique nature of this modality. We build the first unified and largest standardized electromagnetic signal dataset covering multiple signal types and tasks. By exploiting the physical properties of electromagnetic signals, we devise a length adaptive multi-signal packing method and a hardware-aware training strategy that enable efficient use and representation learning from heterogeneous multi-source signals. Experiments show that EMind achieves strong performance and broad generalization across many downstream tasks, moving decisively from task specific models to a unified framework for electromagnetic intelligence. The code is available at: <https://github.com/GabrielleTse/EMind>.

## I. INTRODUCTION

Living in a world surrounded by electromagnetic waves, these invisible yet omnipresent signals carry abundant information and are widely applied in critical fields such as communication, navigation, and environmental perception. The tasks of understanding electromagnetic (EM) signals encompass various aspects, including signal property recognition, target feature identification, interference detection, and waveform reconstruction. These tasks support advanced applications such as dynamic spectrum access and intelligent perception, forming the core capability for intelligent sensing and decision-making in complex electromagnetic environments. They also drive the development of scenarios like intelligent transportation, smart cities, autonomous driving, and the Internet of Things (IoT).

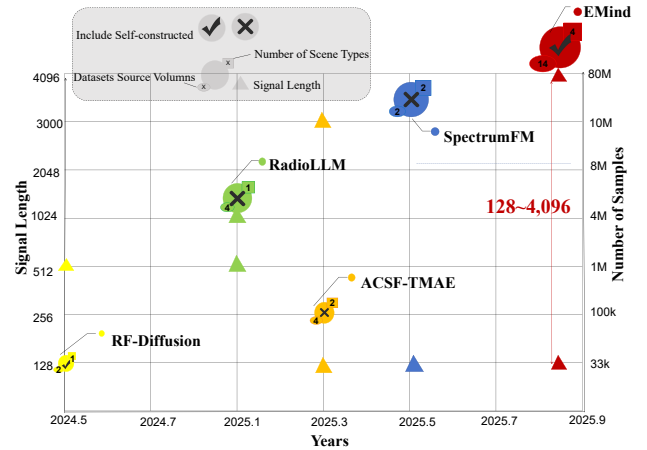


Fig. 2: Comparison of EM signals pre-train datasets: number of samples, data source volume, scene types and signal lengths.

In recent years, deep learning has demonstrated significant advantages in the field of EM signal communication and sensing, driving a shift from traditional rule-based methods and feature engineering toward a data-driven paradigm [1], [2]. However, most existing methods still rely on specialized task-specific models, confronting challenges such as insufficient generalization capabilities and high costs to adapt to new tasks. Therefore, there is an urgent need for a generalized foundation model to enhance the understanding of EM signals across multiple tasks. To support the validation of the pre-training and fine-tuning paradigm on EM signal modalities, it is imperative to construct large-scale datasets. Nevertheless, since most EM signal data originate from non-cooperative scenarios, the protocol standards are generally not public and even subject to encryption protection. This results in existing data being scarce, fragmented, and non-standardized, making the acquisition of high-quality data extremely difficult. Therefore, we have systematically organized and constructed to date the largest unified, standardized EM signal dataset covering multiple signal types and tasks to support large-scale pre-training. As shown in Figure 2, this

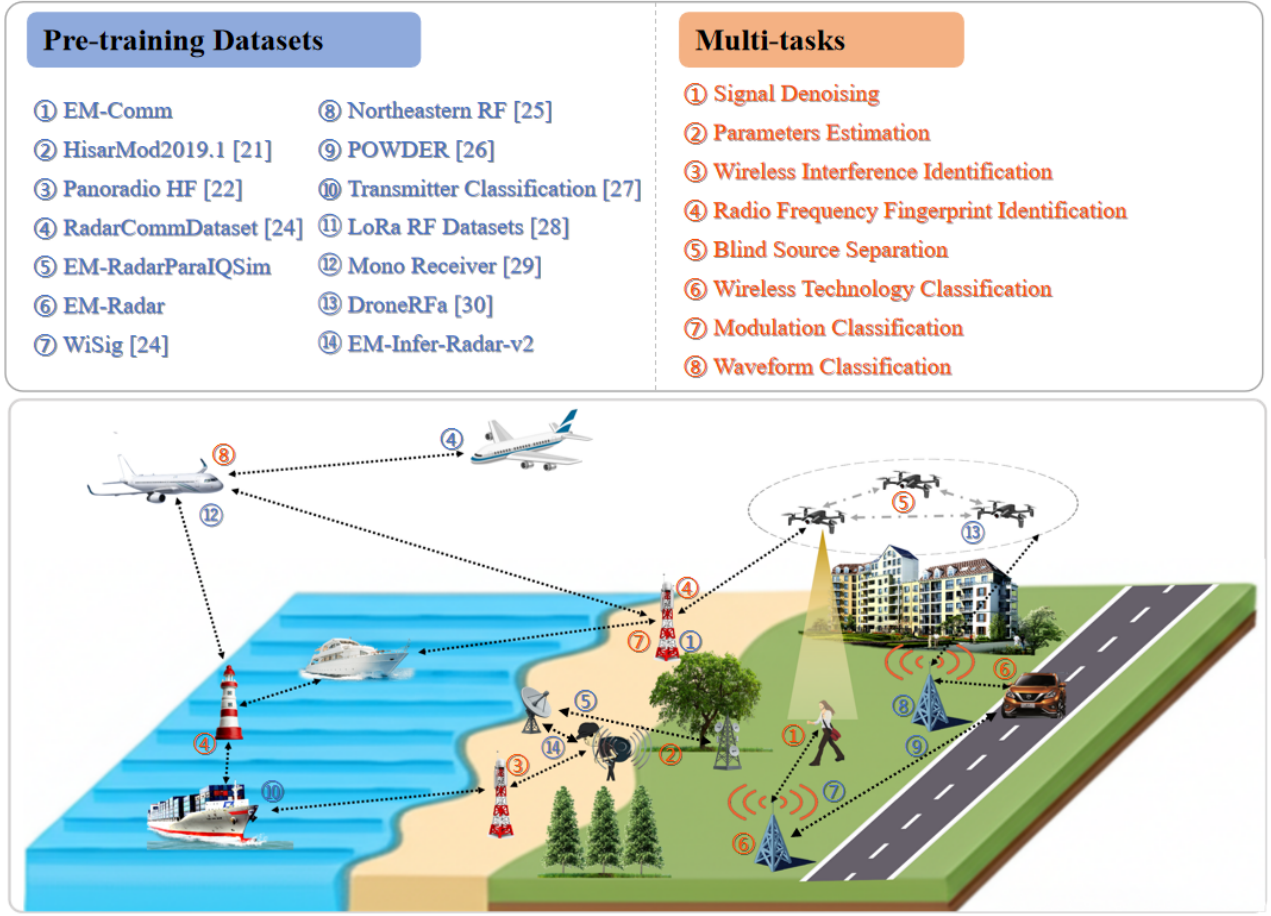


Fig. 1: EMind. A foundation model for electromagnetic signals capable of multitask learning, including signal denoising, parameter estimation, modulation classification and interference identification, applied across diverse fields such as communication, navigation, and security.

dataset provides a firm basis for universal feature representation learning.

While recent efforts have transplanted the foundational-model paradigm from Natural Language Processing (NLP), Computer Vision (CV) [3], and general Time Series (TS) modeling to the field of EM signals, the electromagnetic modality remains fundamentally distinct. RF waveforms exhibit simultaneous sparsity and continuity in the joint time–frequency domain, are inherently non-discrete, and are sourced from a highly heterogeneous space—properties that diverge sharply from tokenized text or 2-D imagery. Naively repurposing existing architectures therefore incurs substantial representational misalignment. To close this gap, we introduce EMind, a foundation model for multi-task learning of communication and sensing on EM signals. EMind’s architecture integrates length-adaptive multi-signal packing with per-sample masking, enabling efficient modeling and robust feature extraction tailored to the physical characteristics of electromagnetic data.

Building upon a unified data foundation and model architecture, we systematically validate the generalizability of the pre-training–fine-tuning paradigm in electromagnetic intel-

ligence. Specifically, a single backbone network is shown to accommodate discriminative tasks such as Automatic Modulation Classification (AMC), Radar Waveform Classification (RWC), Radar Parameter Estimation (RPE), Wireless Interference Identification (WII), and Radio-Frequency Fingerprinting Identification (RFFI), while further extending to high-complexity generative reconstruction tasks including Blind Source Separation (BSS) and Signal Denoising (SD). Crucially, by integrating auto-encoders (AE) into the base model, we demonstrate that in reconstruction-oriented generative scenarios, the model continues to benefit from initialization with pre-trained weights, yielding substantial performance improvements. This observation not only enriches the applicability spectrum of the pre-training–fine-tuning paradigm across electromagnetic signal tasks but also provides new empirical evidence that advances electromagnetic intelligence from specialized models toward a new stage of generalized understanding. In summary, the following main contributions are presented in this paper:

- We present EMind, a purpose-built foundation model for electromagnetic signals that bridges the gap between large-scale pre-training paradigms and the EM signal

modality, establishing a solid basis for superior representation learning.

- We design an architecture tailored to electromagnetic data, introducing a signal discretization mechanism, variable-length input handling, and efficient training strategies for massive heterogeneous datasets, all addressing the unique characteristics of variable sequence length EM signals and the coexistence of temporal sparsity and continuity.
- We construct the largest-to-date EM signal dataset, spanning diverse signal classes, rich attribute labels, and multiple downstream tasks, delivered with unified normalization and high-efficiency storage to create a robust data foundation for large-scale pre-training and universal feature learning.
- EMind systematically demonstrates the broad applicability of pre-train–fine-tune to EM signal tasks, markedly reducing reliance on task-specific designs and setting new SOTA results. Critically, we are the first to adopt reconstruction-oriented fine-tuning for generative tasks such as BSS and SD, empirically showing that pre-trained weights retain their efficacy and thereby extending the paradigm’s frontier.

## II. RELATED WORKS

This section provides a review of existing literature relevant to Foundation Models in communication and sensing, categorized into three key areas: training datasets and method design.

### A. Training Datasets for EM Foundation Models

EM Foundation Models heavily depends on the availability of large-scale, diverse, and high-quality datasets for pre-training [4], [5], [6], [7]. Specifically, the EM foundation models focus on pre-training with extensive wireless datasets to acquire task-agnostic representations. However, collecting such datasets in wireless communication contexts presents unique challenges due to the complex and dynamic nature of radio frequency (RF) environments, which include variations in signal conditions, interference patterns, and propagation characteristics [8], [9].

To construct reliable dataset, most EM foundation models development has historically leveraged synthetic or simulated data. For instance, WirelessGPT [10] was pre-trained on a large-scale wireless channel dataset, encompassing both publicly available and self-developed datasets like Traciverse, SionnaRT [11], and DeepMIMO [12]. Similarly, WiMAE [9] utilized the DeepMIMO dataset to generate over a million channel samples for pre-training across various scenarios. While simulated datasets offer control and scalability, they may not fully capture the intricacies and unpredictable variabilities of real-world EM environments.

To enhance the quality of pre-training datasets, some studies incorporate real-world data. For example, WavesFM [13] was pre-trained solely on real-world data, including Radio Frequency (RF) spectrograms, WiFi Channel State Information (CSI) samples, and 5th Generation (5G) CSI samples

collected from diverse geographical locations and scenarios. Additionally, SpectrumFM [14], a foundation model for intelligent spectrum management, compiled a comprehensive dataset from various sources, including publicly available open-source datasets like RML2018.01A [15] and TechRec [16], as well as signals collected in real-world practice scenarios. These efforts highlight a shift towards more realistic and diverse data sources to build robust and universally applicable EM Foundation Models.

The performance of foundation models is significantly impacted by their pre-training datasets. However, datasets utilized in prior work often exhibit limitations in terms of diversity and volume, consequently constraining the models’ generalization capabilities on downstream tasks.

### B. Design of Foundation Models towards Electromagnetic Signals

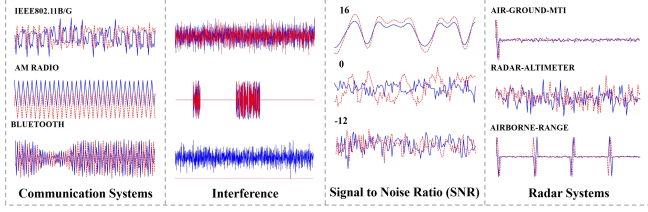
The architectural design of EM Foundation Models is crucial for effectively capturing the complex spatio-temporal and frequency correlations inherent in wireless data, and for enabling efficient multi-task learning [17], [18], [19].

Inspired by the success of transformer architectures in Natural Language Processing (NLP) and Computer Vision (CV), many EM foundation models adopt similar principles [20], [10], [9]. For instance, WirelessGPT [10] employed a Transformer-based foundation model to capture spatial, temporal, and frequency correlations in wireless channel data. Similarly, WavesFM [13] utilized a Vision Transformer (ViT)-based architecture that learns rich wireless signal representations via self-supervised learning, particularly through a Masked Wireless Modeling (MWM) approach. Furthermore, some research focuses on enhancing architectural design for signal data. For instance, SpectrumFM [14] introduced a novel hybrid encoder architecture that synergistically combines Convolutional Neural Networks (CNNs) for localized feature extraction with Multi-Head Self-Attention (MHSA) mechanisms.

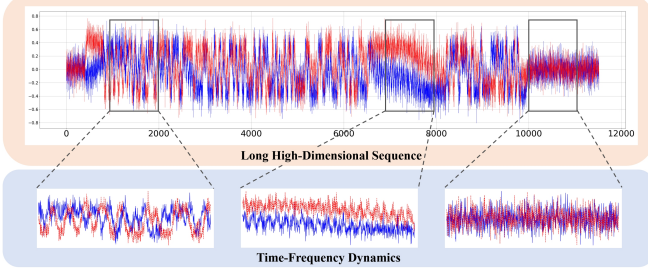
Beyond architectural design, some works explore diverse pre-training methodologies. For instance, WiMAE [9] adopted masked signal reconstruction for pre-training. Furthermore, ContraWiMAE [9] extended this approach by incorporating a contrastive learning objective to enhance discriminative feature learning. In addition to masking-based pre-training, some methods utilize hybrid pre-training strategies. For example, SpectrumFM [14] was pre-trained via two self-supervised learning tasks: masked reconstruction and next-slot signal prediction. This approach enables the model to learn latent structures and intrinsic correlations, thereby improving its feature extraction capabilities and robustness.

However, the disparate data formats and scales across various datasets limit the data utilization efficiency of the aforementioned studies.

### III. PROBLEM FORMULATION AND CHALLENGES



(a) Diverse signal types with intricate semantics exhibit a wide spectrum of characteristics.



(b) Long high-dimensional signals show time-frequency dynamics.

Fig. 3: Visualization of signals exhibits their heterogeneous and complicity.

Electromagnetic signals constitute a specialized class of time-series data, typically emitted by electromagnetic sources such as communication stations and radar systems. After propagating through the wireless medium, these signals are received and processed by the receiver front-end, where they undergo analog operations including downconversion and low-pass filtering to obtain the baseband signal. The resulting baseband signal is then represented in complex form as in-phase and quadrature (IQ) samples. This IQ representation, which preserves both amplitude and phase information of the original waveform, serves as the canonical digital form of EM signals at the receiver side. Specifically, a real-valued EM signal  $x(t)$  with a carrier frequency  $f_c$  can be expressed as:

$$x(t) = I(t) \cos(2\pi f_c t) - Q(t) \sin(2\pi f_c t), \quad (1)$$

where  $I(t)$  and  $Q(t)$  represent the in-phase and quadrature-phase components of the signal, respectively. The baseband signal can be further discretized with a sampling rate  $f_s$ , resulting in a discrete IQ sequence, which is,

$$s[n] = I[n] + jQ[n], \quad n = 0, 1, 2, \dots, N-1. \quad (2)$$

Here,  $n$  represents the length of the sequence. As the complexity of the electromagnetic environment continues to increase, the types and quantity of electromagnetic signals are rapidly growing. Due to the significant differences in the characteristics and objectives of various tasks, single-task learning models perform poorly in cross-task generalization and have low training efficiency. Therefore, there is an urgent need to learn discriminative representations that capture general features to enhance the generalization ability of downstream tasks. However, developing such a foundational model for EM signals still faces the following challenges:

**Challenge 1: Constructing a unified pre-training dataset for electromagnetic signals.** EM signals are diverse, and their modulation methods and propagation characteristics exhibit significant heterogeneity, which makes the semantic structure of EM signals exceptionally complex, containing both short-term transient features and long-range dependencies. Additionally, under high bandwidth or long time-window observation conditions, EM signals tend to generate extremely long high-dimensional sequences (as shown in Figure 3). Therefore, constructing a pretraining dataset that covers multiple signal types faces challenges in data selection, alignment, and standardization. It is essential to ensure that these signals share a common foundation, so that effective training becomes possible.

**Challenge 2: Developing an effective model architecture toward electromagnetic signals.** EM signals, as a unique modality, exhibit significant semantic differences between different types of signals. Each signal stage typically carries semantic information related to specific tasks. Therefore, designing a network architecture that can both account for the physical properties of EM signals and effectively express their semantic information, while efficiently applying the pretraining-finetuning strategy, presents a major challenge in constructing a foundation model suitable for EM signals.

### IV. DATASET

The dataset construction pipeline is as follows: multi-source datasets from communications, radar, radio frequency, and interference domains are systematically integrated, with all signals saved in their raw IQ (in-phase and quadrature) format. To ensure data quality and enable unified large-scale pretraining, data cleansing is performed on the raw data; detailed parameter recording and labeling are completed by domain experts, and the data are uniformly converted into an  $n \times 2$  dimensional format and stored as Parquet files. In addition, quality validation is conducted through randomized visual inspections. Through this series of stringent procedures, the largest known EM signal dataset for machine learning applications is ultimately constructed, as shown in Figure 4.

#### A. Source Screening

The dataset we constructed comprises a wide variety of signal types, with the core principle being the maximization of signal and task diversity to ensure both the breadth and effectiveness of the training data. To achieve this, we systematically curated multiple publicly available signal datasets and supplemented the public data with self-collected data to address missing categories or insufficient samples. As shown in Table I, our pretraining dataset consists of 14 datasets, covering a wide range of acquisition devices, signal types, signal lengths, sampling rates, and other factors. Of these, 10 are publicly available databases, totaling 77,622,845 samples, while the remaining four datasets are self-collected (bolded in the table, prefixed with 'EM-'), totaling 3,494,680 samples. It is worthy to note that, even for the publicly

TABLE I: EM Pre-train Dataset. Bold indicates self-collected data, the others are publicly available datasets.

Dataset Name	Transmitter	Receiver	Signal Type	Signal Length	Sampling Rate	Data* Source	Number of Samples
<b>EM-Comm</b>	<b>a USRP X310</b>	-	<b>Category 14 modulated signals, SNR: -20~-18db</b>	<b>1,024</b>	<b>20 MHz</b>	<b>Real-world</b>	<b>2,747,000</b>
HisarMod2019.1 [21]	-	-	Category 26 modulated signals, SNR: -20~-18db	1,024	1 MHz	Simulation	780,000
Panoradio HF [22]	-	-	Category 18 modulated signals, SNR: -10~-25d	2,048	6 kHz	Simulation	172,800
RadarCommDataset [23]	a USRP N210	USRP N210	Category 6 modulated signals, Category 8 signal types, SNR: -20~-18db	128	10 MHz	Real-world & Simulation	860,361
<b>EM-RadarParaIQSim</b>	-	-	<b>Category 2 radar types, Category 3 parameters, SNR: 6~-12db</b>	<b>320/384 400/480</b>	<b>10/12 MHz</b>	<b>Simulation</b>	<b>300,000</b>
<b>EM-Radar</b>	-	-	<b>10 radar emitters, including 5 radar waveforms, and 3 radar system parameters SNR: -10~-20db</b>	<b>1,024</b>	<b>5 MHz</b>	<b>Simulation</b>	<b>327,680</b>
WiSig [24]	174 WiFi Emitter	41 USRP B210/N210/X310	IEEE802.11a/g	256	25 MHz	Real-world	18,243,630
Northeastern RF [25]	20 USRP devices	-	IEEE802.11a/g	288	20 MHz	Real-world	17,930,880
POWDER [26]	4 USRP X310	USRP B210	5G, WiFi, LTE	512	5/7.68 MHz	Real-world	1,044,472
Transmitter Classification [27]	21 USRP devices	USRP N2932	IEEE 802.15.4	600	5 MHz	Real-world	11,928,835
LoRa RF Datasets [28]	25 Pycom devices	USRP B210	LoRa	4,096	1 MHz	Real-world	13,498,730
Mono Receiver [29]	Over 140 civil aircrafts	USRP B210	ADS-B	974	8 MHz	Real-world	30,367
DroneRFa [30]	24 categories of UAVs	USRP	Communication RF	1,024	100 MHz	Real-world	13,132,770
<b>EM-Infer-Radar-v2</b>	-	-	<b>Category 12 radar interference types ISR: 30~-60db</b>	<b>2,048</b>	<b>20 MHz</b>	<b>Simulation</b>	<b>120,000</b>
TOTAL							<b>81,117,525</b>

available datasets, we conducted thorough selection and pre-processing. Ultimately, the total volume of our pretraining dataset reaches 81,117,525 samples, making it the largest known EM signal pretraining dataset to date. Detailed dataset configurations can be found in the Appendix.

### B. Expert Annotations

For the annotation of EM signals, the ground truth labels for publicly available datasets are typically provided by the original data publishers. In the case of simulation datasets, the labels are automatically generated during the data generation process, based on predefined modulation schemes, channel parameters, or radar waveform configurations. For self-collected datasets, the labels are controlled by the data acquisition process, usually generated based on information recorded by the experimenters, such as device types, sampling distances, frequency bands, modulation types, and signal strength. Based on these principles, we have standardized 17 key attributes: iq data, dataset name, sampling rate, device id, transmission id, infer class, signal-to-noise ratio (SNR), interference-to-signal ratio (ISR), modulation type, radar waveform type, pulse repetition interval (PRI), pulse time delay, number of pulses, pulse width, band width,

amplitude, and radar segmentation type. If a specific dataset lacks one or more of these fields, the corresponding entries are assigned a default value of None.

### C. Quality Control

To ensure the integrity of the data and its relevance to the task, a reliable quality control process has been established. First, IQ data is randomly sampled from the dataset, with all parameters printed and waveforms plotted. This process involves checking the data format and content, considering factors such as sampling rate and amplitude range, while also inspecting for issues such as anomalous padding. Any anomalies or discrepancies discovered are marked and submitted for expert review. After identifying the cause, erroneous data is either corrected or regenerated to ensure accuracy. This closed-loop quality control mechanism enables the continuous optimization of the dataset, effectively ensuring the overall reliability of the data.

### D. Analysis

Our pre-training dataset exhibits pronounced advantages in terms of scene diversity, signal length, and data volume. It encompasses four principal operational scenarios (communication, radar, radio frequency and interference), eight

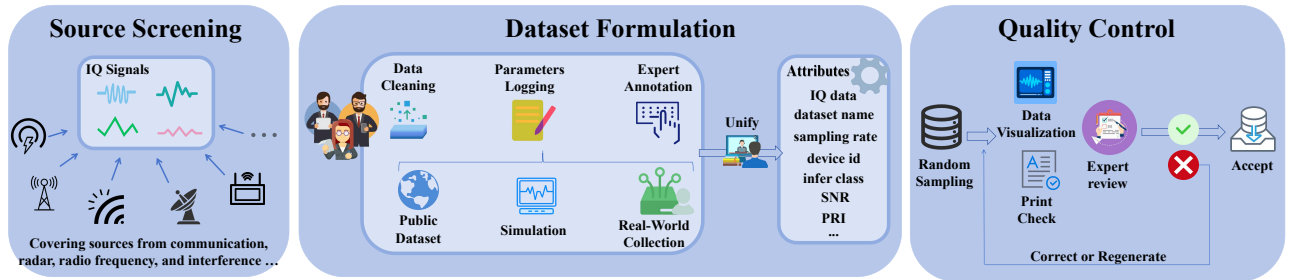


Fig. 4: Pipeline of EM pre-train dataset construction. Our pipeline comprises 3 stages all led by experts: Source Screening, Dataset Formulation, and Quality Control.

TABLE II: Comparison of pre-train datasets

Pre-train Dataset	Dataset Source Volumn	Include Self-constructed	Signal Length	Scene Type	Number of Samples
RF-Diffusion [31]	2	✓	512	radio frequency	33 k
ACSF-TMAE [32]	4	×	128 & 3,000	communication & radio frequency	1 million
RadioLLM [33]	4	×	128 & 1,024	communication	4 million
SpectrumFM [14]	3	✓	128	communication & radio frequency	8-10 million*+ 25 GB <sup>†</sup>
EMind	14	✓	128~4096	communication & radar & radio frequency & interference	81 million

\* In [14], the pre-training data volume for TechRec is estimated according to <https://github.com/JaronFontaine/Technology-Recognition-dataset-of-real-life-LTE-WiFi-and-DVB-T?tab=readme-ov-file>

<sup>†</sup> 25GB is a self-collected dataset without length unspecified.

TABLE III: Main statistics of our dataset

Statistic	Number of Samples
Task type	
- Communication	3,699,800
- Radar	1,488,041
- Radio frequency	75,809,684
- Interference	120,000
Attributes	
- Modulation	4,560,161
- Radar Waveform	627,680
- Signal-to-Noise Ratio (SNR)	5,218,208
- Interference class	120,000
- Interference-to-Signal Ratio (ISR)	120,000
- Band width	327,680
- Pulse repetition interval (PRI)	627,680
- Pulse width	627,680
- Device id	75,809,684
- Transmission id	17,930,880
Signal Length	
- 128	860,361
- 256	18,243,630
- 288	17,930,880
- 320	75,000
- 384	75,000
- 400	75,000
- 480	75,000
- 512	1,044,472
- 600	11,928,835
- 974	30,367
- 1,024	16,987,450
- 2,048	292,800
- 3,840	12,399
- 4,096	13,498,730

distinct signal modalities (Airborne detection radar, Airborne range radar, Air-Ground MTI radar, Ground mapping radar, Radar Altimeter, SATCOM, AM Radio, Short-range wireless), twenty-nine modulation formats (BPSK, QPSK, 8PSK,

16PSK, 32PSK, 64PSK, 4QAM, 8QAM, 16QAM, 32QAM, 64QAM, 128QAM, 256QAM, 2FSK, 4FSK, 8FSK, 16FSK, 4PAM, 8PAM, 16PAM, AM-DSB, AM-DSB-SC, AM-USB, AM-LSB, FM, PM, morse, psk31, psk63), nine radar waveforms Coherent Pulse Train, Barker Code, Polyphase Barker Code, Frank Code, Linear Frequency Modulated (LFM), Rectangular, Phase Coded, Stepped FM and Custom FM), and twelve interference classes (Pure Noise, Intermittent Sampling Forwarding Interference, Spot-Jamming Interference, Blocking Interference, Frequency-Sweeping Interference, Range-Fooling Interference, Dense False Target Interference, Smart Noise Interference, Chaff Interference, Chaff Interference Combined with Intermittent Sampling Forwarding Interference, Dense False Target Interference Combined with Smart Noise Interference, and Range-Fooling Interference Combined with Frequency Modulated Frequency-Sweeping Interference). Furthermore, the dataset accommodates signal lengths spanning 128 to 4,096 sampling points. A comparative summary against other available pre-training dataset is provided in Table II and Figure 2.

1) *Diversity of task types*: Our dataset includes a variety of task types, including communication datasets EM-Comm, HisarMod2019.1, and Panoradio HF; radar datasets RadarCommDataset, EM-RadarParaIQSim, and EM-Radar; interference dataset EM-Infer-Radar-v2; and wireless RF datasets WiSig Raw, Northeastern RF, POWDER, Transmitter Classification, LoRa RF Datasets, Mono Receiver, and DroneRFa, covering a wide range of protocols and devices from WiFi, LoRa to ADS-B, UAV, and more.

2) *Comprehensive annotations*: We provide detailed annotation information for the dataset, including the modulation type of communication signals; waveform type, pulse width and pulse repetition period for radar signals; device id and bandwidth for RF signals; and interference type and interference-to-signal ratio (ISR) for interference signals. All data are annotated with sampling rate, which typically ranges from kilohertz (kHz) to several hundred megahertz (MHz), a critical attribute for processing EM signals. Additionally,

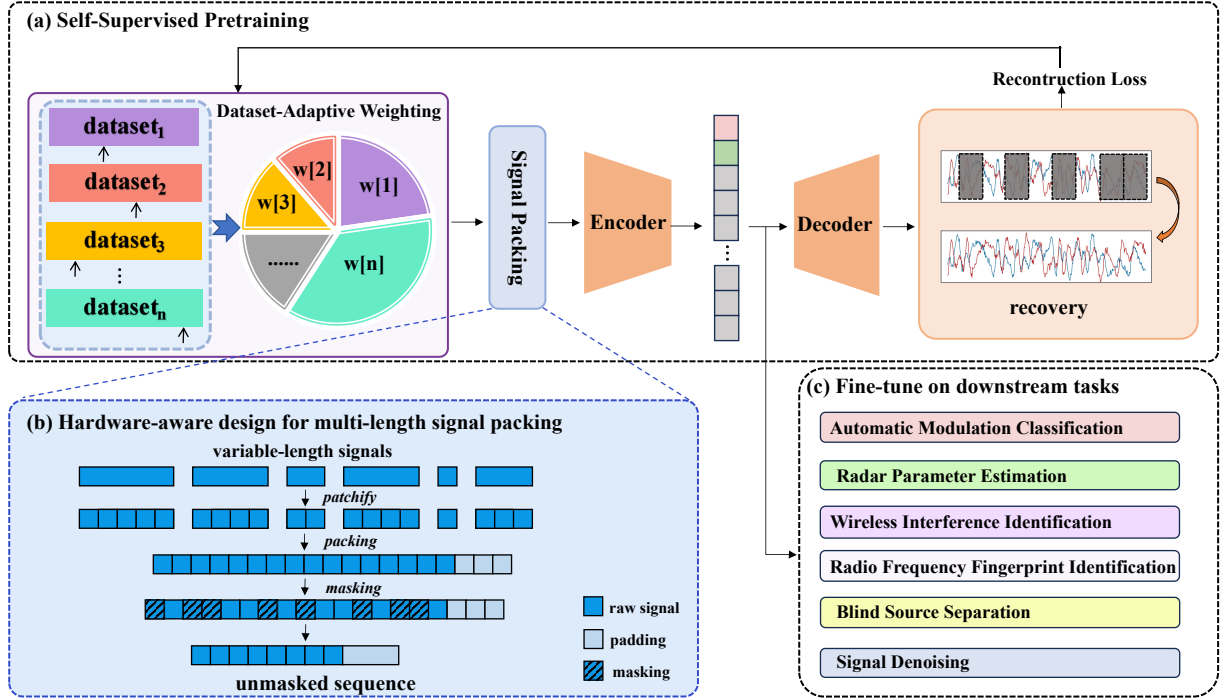


Fig. 5: EMind (a) Large-scale multi-scenario self-supervised pre-training with dataset-adaptive weighting. (b) Low-redundancy length adaptive multi-signal packing and per-sample masking. (c) Fine-tune on multiple downstream tasks with support for arbitrary-length signal inference.

all available data are annotated with Signal-to-Noise Ratio (SNR). These comprehensive annotations ensure the high quality and completeness of the dataset.

3) *Length of Samples*: Our pre-training dataset covers signal lengths ranging from 128 to 4,096 samples, which enables the model to train on a wider range of dataset. As detailed in Table II, existing datasets are typically restricted to a single operational scenario or composed of fixed-length signals. Our flexible signal-length design enables the potential for arbitrary length inference, allowing the model to better adapt to complex signals of varying durations. Such variability markedly improves generalization to real-world data, allowing the network to robustly capture both transient features and long-range dependencies across diverse EM signals; detailed statistics are provided in Table III.

## V. EMIND: ELECTROMAGNETIC SIGNAL FOUNDATION MODEL

To address the fundamental challenge of high heterogeneity and semantic complexity inherent in EM signals, we propose to implement a unified pre-training and fine-tuning paradigm, as shown in Fig. 5 (a). Concretely, we first adopt a Transformer encoder-decoder architecture and perform Masked Auto-Encoding (MAE) on massive unlabeled multi-scenario IQ streams. By imposing an aggressive masking ratio of 75 %, the model is forced to reconstruct the IQ signal under extreme information scarcity, thereby learning modulation- and channel-agnostic universal continuous-sparse representations. In the subsequent downstream

fine-tuning stage, a task-specific head is fine-tuned. This two-stage strategy projects intricate transient semantics, steady-state characteristics, and heterogeneous modulation discrepancies into a shared high-dimensional manifold, enabling rapid adaptation with minimal labels and robust cross-domain generalization for high-quality multi-task EM signal modeling.

To handle the dynamic and long-sequence nature of EM signals, we propose a packing strategy that supports variable-length inputs, as illustrated in Fig. 5(b). Specifically, we first concatenate multiple IQ samples of varying lengths into a single ultra-long sequence, enabling efficient joint training across different lengths. This mechanism also allows flexible processing of inputs of any length during inference. Detailed implementation is provided in Section V-B.

### A. IQ tokenizer

Faced with the highly heterogeneous nature of EM signals due to their varied types, diverse scenarios, multiple tasks, differing sampling rates, modulation schemes and channel conditions, we present a pipeline of discretization, tokenization and embedding. The continuous yet sparse IQ stream is divided evenly into local patches that preserve the phase amplitude coupling while greatly shortening the sequence length. An IQ tokenizer maps each patch into a high dimensional sample token through an embedding by concatenating the embedded sampling rate. Finally a one dimensional temporal Transformer, specifically designed for IQ structures, aggregates local and global contextual features.

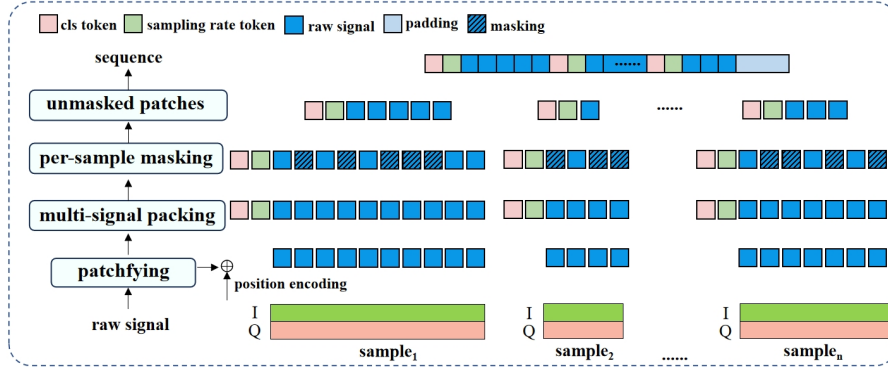


Fig. 6: Low-redundancy length adaptive multi-signal packing and per-sample masking. Multiple signal samples are dynamically packed into fixed-length sequences, followed by per-sample masking strategy.

Sampling rate is an intrinsic, stable meta-attribute that spans kHz–MHz across datasets. Each signal is prefixed with both a dedicated sampling-rate token and the standard classification token. The two are functionally isolated and differentiated solely by positional encodings: the classification token yields a global representation, whereas the sampling-rate token is left unmasked and always visible. During reconstruction, the model therefore continuously perceives the acquisition rate of each signal, naturally aligning itself with sampling-rate-sensitive tasks—such as pulse-width, PRI, or bandwidth regression—without further scaffolding.

### B. Low-Redundancy Length Adaptive Multi-Signal Packing

To enable adaptive processing of signals with varying lengths, and to support unified training with long samples in a memory-efficient manner, we propose a novel variable-length signal packing strategy as an alternative to conventional batch padding. Our training data is sourced from multiple heterogeneous datasets, exhibiting significant variation in signal lengths—from 128 to 4,096—spanning a  $32\times$  range. Under such highly non-uniform length distributions, traditional padding leads to excessive zero-padding, resulting in substantial memory overhead and computational inefficiency, which severely limits training scalability and hardware utilization. To address this, we design a dynamic packing mechanism that predefines a maximum sequence length as the capacity for each packed sequence. Incoming IQ samples are sequentially inserted until the remaining capacity is insufficient, at which point a new sequence is initiated. To ensure that the model can accurately distinguish and focus on individual signals—preventing interference and information leakage across samples—we record the boundary indices of each sample within the packed sequence. This preserves information integrity and enables efficient signal utilization. Compared with traditional padding-based approaches, our packing strategy effectively mitigates the computation redundancy and memory bottlenecks caused by zero-padding, providing a practical and scalable solution for large-scale pretraining.

Given the large scale of the pre-training corpus, even with the multi-signal packing, each epoch must still process a

massive number of samples. To address this, we design an asynchronous data loading and training coordination system. A unified buffer is allocated on the CPU side, where data is organized asynchronously based on a producer-consumer model. The CPU is responsible for parallel data loading, preprocessing, and buffer management, while a streaming scheduling mechanism enables tight coordination between the CPU and GPU. This forms a concurrent asynchronous pipeline that allows data acquisition and model training to proceed in parallel, thereby maximizing memory utilization. With this efficient architecture, we are able to process up to 81 million samples within a single epoch, resulting in significant improvements in training throughput and resource utilization.

Moreover, the proposed EMind is designed with strong modularity and scalability. By flexibly switching the downstream task head, the shared pre-trained foundation model can be adapted to various task types, including classification, regression, detection, and separation, as shown in Fig. 5 (c). Benefiting from our flexible packing method, the model naturally supports arbitrary-length signal inputs during inference, thereby balancing computational efficiency with input diversity.

### C. Per-Sample Masking in Multi-Signal Packing

We face a critical challenge in mask control for packed EM signal sequences: existing masking strategies typically operate on the entire concatenated long sequence. Since the sequence contains multiple signal samples of varying lengths mixed together, the precise boundaries of individual samples cannot be distinguished. As a result, the effective masking ratio fluctuates significantly across the overall sequence. For example, shorter signals may be fully masked while longer signals receive insufficient masking. This directly impacts the stability and generalization ability of model training, making it difficult to achieve balanced masking on a per-sample basis.

To address the above issue, we designed and implemented an efficient per-sample masking algorithm. The core idea is to accurately record and utilize the boundary information of each signal sample, performing independent random

shuffling and mask sampling within each sample. Although previous implementations based on explicit loops could apply mask control on a per-sample basis, they significantly increased computational complexity, undermining the efficiency of the pipeline’s sequence packing strategy. Therefore, we innovatively propose a masking control mechanism based on vectorized operations that requires no explicit looping.

Specifically, for each signal sample of length  $l$ , we first insert a sampling rate encoding token at the beginning of the sample, concatenated together with the classification token. Next, we normalize the positions of each sampled point within the signal to the interval  $[0, 1]$ , forming an evenly spaced position coordinate set:

$$\left\{ \frac{1}{l-1}, \frac{2}{l-1}, \dots, 1 \right\}. \quad (3)$$

Using this normalized positional information, the signal points inside each sample are randomly shuffled. Then, according to the predefined masking ratio, a selective subset of valid patches is chosen from the shuffled sample data for model training. This approach effectively guarantees that a fixed proportion of content within every individual signal is masked evenly, ensuring consistent and fair mask application regardless of signal length variability, thereby avoiding mask ratio fluctuations.

It is worth noting that our masking scheme specially considers the unique status of the sampling rate token by keeping its position fixed and always included during training. As an intrinsic meta-information token for each sample, the sampling rate token is neither masked nor involved in the random shuffling, which ensures the model consistently captures key information about the signal’s sampling rate, enhancing sensitivity and recognition of its time-frequency characteristics during training. Based on the above mechanism, the model only needs to perform forward propagation on the unmasked valid patches during training, drastically reducing redundant computation and significantly improving overall computational efficiency and training speed, as illustrated in Figure 6.

#### D. Hardware-aware Dataset-adaptive Weighting

The proposed hardware-aware training framework not only provides efficient computational support for large-scale pre-training on heterogeneous EM signals, but also addresses key challenges such as significant difficulty variance across data sources and imbalanced convergence speeds. To this end, we further design a dataset-adaptive weighting mechanism. Specifically, the system initializes with an equal-weight sampling strategy (i.e., 1:1:1:...) across all datasets as the training baseline. During training, it continuously monitors the evolution of training and validation losses for each dataset. By analyzing the loss trajectories, the system identifies datasets that exhibit slow convergence or signs of performance degradation (e.g., overfitting or catastrophic forgetting). The sampling weights of such datasets are then increased dynamically to enhance the model’s learning on more challenging samples, while the sampling frequency

of easily-learned or overfitting-prone datasets is reduced accordingly to mitigate overfitting and maintain training stability and generalization.

To implement this strategy, we introduce a precise sampling weight control mechanism within the buffer. Leveraging a memory-mapped sequential access strategy, the system ensures that samples of varying difficulty levels or classes are drawn in each training batch according to the target sampling weights. Concretely, each dataset is assigned an independent pointer whose movement speed is adjusted based on the current target sampling weight. These speeds are updated in real time according to the latest weight assignments, ensuring that each batch contains a mixture of samples that reflects the dynamically adjusted proportions. This mechanism not only strengthens the model’s focus on hard-to-learn samples but also suppresses excessive reliance on subsets prone to overfitting. The used sampling weights for each dataset in this pre-training are detailed in Section VI-A.1.

## VI. EXPERIMENTS

In this section, we aim to comprehensively validate the effectiveness and generalizability of the proposed EMind across a variety of EM signal tasks. We begin by detailing the pre-training setting, including training strategy and model specifications. Subsequently, we conduct downstream evaluation experiments on several representative tasks to systematically assess the model’s capability in EM feature representation, cross-task transferability, and few-shot generalization.

### A. Pre-training setting

1) *dataset weight of training strategy*: During the pre-training process, all pre-training datasets are split into training and validation sets in a 9:1 ratio, with data having an SNR greater than 6 selected for pre-training. We propose a library-level real-time self-supervised reconstruction loss tracking mechanism, which dynamically adjusts the sampling ratio based on training iterations. This mechanism reduces the sampling ratio for datasets prone to overfitting and increases the ratio for harder-to-learn datasets, thereby enhancing the model’s ability to model features from difficult subsets and improving its overall generalization performance. Ultimately, the sampling ratios for our pre-training datasets are set as follows, EM-Comm : HisarMod2019.1 : Panoradio HF : RadarCommDataset : EM-RadarParaIQSim : EM-Radar : WiSig : Northeastern RF : POWDER : Transmitter Classification : LoRa RF Datasets : Mono Receiver : DroneRFa : EM-Infer-Radar-v2 = 1 : 0.5 : 1 : 1 : 0.5 : 0.5 : 1 : 1 : 1 : 1 : 1 : 1 : 0.5 : 0.5. The pre-training process is completed within 24 hours over 10 epochs. The final pre-trained weights used for downstream tasks are passively selected from the checkpoint at the end of the 3.6-th epoch, due to its empirically observed training stability and generalization performance.

2) *Model specifications*: The hyperparameter configuration for pretraining is as follows: the mask ratio is set to 75 %, the encoder has 12 layers and the decoder has 8 layers; the optimizer is AdamW with a base learning rate of 1e-4

TABLE IV: Multi-task Dataset

Dataset	Task Type*	Number of Types	Signal Length	Sampling Rate (Hz)	SNR Range (dB)	Data Source
RML2016.10A [34]	AMC	11	128	1M	[-20:18]	-
RML2016.10B [34]	AMC	10	128	1M	[-20:18]	-
RML2016.04C [35]	AMC	11	128	1M	[-20:18]	-
RML2018.01A [15]	AMC	24	1024	1M	[-20:30]	-
RadChar [36]	RWC/RPE	5	512	3.2M	[-20:20]	-
ADS-B [37]	RFFI	198	3000	50M	-	-
<b>EM-AIS</b>	RFFI	112	3,840	156.25M	-	Real-world
<b>EM-Infer-Comm</b>	WII	9	1,024	20M	[-20:20]	Simulation
<b>EM-Infer-Radar</b>	WII	12	1,024	20M	[-20:20]	Simulation
<b>EM-Radar-Mix</b>	BSS	-	1,024	5M	12	Simulation
<b>EM-Denoise-Signal</b>	SD	-	1,024	20M	[-3:20]	Simulation

\* AMC represents Automatic Modulation Classification; RWC refers to Radar Waveform Classification; RPE stands for Radar Parameter Estimation; WII denotes Wireless Interference Identification, RFFI indicates Radio Frequency Fingerprint Identification; SD refers to Signal Denoising; and BSS denotes Blind Source Separation.

TABLE V: Classification results compared with State-of-the-art. BOLD indicates the best performance.

TASK	AMC				RFFI		WII	
METHOD	RML2016.10A*	RML2016.10B*	RML2016.04C*	RML2018.01A	ADS-B	EM-AIS	EM-Infer-Comm	EM-Infer-Radar
ResNet [38]	50.04	54.88	55.97	43.06	84.51	42.02	76.79	71.64
MCNet [39]	53.52	59.22	59.57	-	-	-	-	-
CNN2 [15]	53.25	57.14	59.45	-	-	-	-	-
GRU2 [40]	58.80	64.11	63.13	-	-	-	-	-
DAE [41]	58.97	61.46	55.91	-	-	-	-	-
CGDNN [42]	56.57	58.26	60.34	-	-	-	-	-
Transformer [20]	59.27	63.10	65.41	59.45	78.77	39.12	80.44	77.05
MSNet [43]	58.33	63.49	63.66	-	-	-	-	-
AMC_Net [44]	59.10	63.38	63.01	-	-	-	-	-
SpectrumFM [14]	63.72	65.35	73.37	-	-	-	-	-
EMind	62.51	<b>65.45</b>	<b>74.34</b>	<b>63.83</b>	<b>99.87</b>	<b>57.07</b>	<b>81.70</b>	<b>79.19</b>

\* As stated in the scikit-learn documentation ([https://scikit-learn.org/stable/modules/generated/sklearn.metrics.recall\\_score.html](https://scikit-learn.org/stable/modules/generated/sklearn.metrics.recall_score.html)), weighted recall is equivalent to accuracy in single-label multiclass settings. Therefore, we treat the recall reported in [14] as overall accuracy (OA) for RML2016.10A, RML2016.10B, and RML2016.04C.

and a warmup ratio of 10 %; training is carried out for 10 epochs with a batch size of 40 and a maximum sequence length of 6 000; only samples whose signal-to-noise ratio exceeds 6 are used, eager attention is employed, the patch size is fixed at 8, and the final model reaches 110 million parameters.

The IQ data are normalized using absolute magnitude normalization. Considering the physical characteristics of EM signals, the magnitude often directly reflects the signal's strength and energy distribution. Applying absolute magnitude normalization helps preserve this critical feature, thereby enhancing the model's ability to perceive the physical properties of the signal, which is  $\mathbf{IQ} = \mathbf{IQ}/(\max(|\mathbf{IQ}|))$ . The regression parameters are also normalized, particularly when dealing with small time values (such as radar parameters in  $\mu$ s), to improve the training performance and convergence of regression tasks. For radar parameters, min-max normalization is applied.

### B. Downstream tasks

A core feature of the foundational model is its ability to generalize across pretraining data distributions and adapt to a

wide range of downstream tasks. To evaluate this capability, we select a set of fine-tuning datasets that are completely independent from the pretraining datasets, and design four challenging downstream tasks to comprehensively assess the model's performance in electromagnetic application scenarios. As shown in Table IV, the tasks include Automatic Modulation Classification (AMC), Radar Waveform Classification (RWC), Radar Parameter Estimation (RPE), Wireless Interference Identification (WII), Radio Frequency Fingerprint Identification (RFFI), as well as Signal Denoising (SD) and Blind Source Separation (BSS), with the details of these datasets provided in the Appendix. In our model design, all downstream tasks (including classification, regression, and reconstruction) are unified within the same structure, without the need to modify the model's main architecture. During fine-tuning, IQ samples are input directly, allowing for inference at signal-to-noise ratios as low as -20 dB and with sequence lengths up to 6,000. This ensures consistency and scalability when handling samples of varying lengths, enabling a comprehensive evaluation of the model's generalization, adaptability, and robustness in EM signals.

We design three experimental tracks, each corresponding

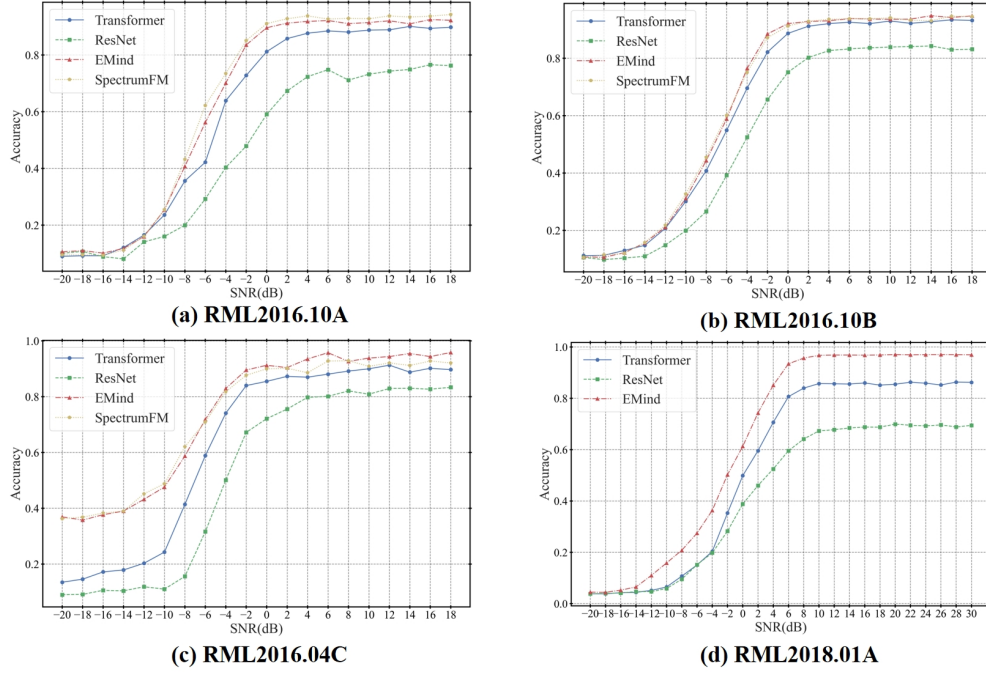


Fig. 7: Performance comparison across different datasets in terms of accuracy at varying signal-to-noise ratios (SNR). (a)-(d) show the results for RML2016.10A, RML2016.10B, RML2016.04C, and RML2018.01A datasets, respectively.

to a different capability dimension of the model. First, in the full fine-tuning setting, all parameters of the model are updated during training to evaluate its adaptability and performance upper bound under fully supervised conditions, thereby validating its effectiveness as a general-purpose model. Second, the linear probe experiment freezes the parameters of the foundation model and trains only a linear classifier on top, in order to assess the general representation capability learned during pre-training and to evaluate the model's effectiveness as a feature extractor. Third, the few-shot Learning setting simulates real-world scenarios with limited labeled data, where the model is fine-tuned with only a few samples per class. This track is used to evaluate the model's transferability and data efficiency under low-resource conditions.

To systematically and comprehensively evaluate the model's performance, we introduce multiple evaluation metrics covering quantitative analysis across different task dimensions, including classification, regression, and blind source separation. In classification tasks, we use Overall Accuracy (OA) to measure overall classification performance. OA represents the ratio of correctly predicted samples to the total number of samples, reflecting the average classification accuracy of the model across all test samples. It is a commonly used and intuitive metric for classification performance. In regression tasks, we adopt Mean Absolute Error (MAE) as the primary metric, which is defined as the average of the absolute differences between the predicted and actual values, effectively measuring the magnitude of the deviation between the model's predictions and the true values. For blind source separation and signal denoising tasks, we

use Signal Distortion Ratio (SDR), Signal Interference Ratio (SIR), Signal Artifacts Ratio (SAR), and Scale-Invariant Signal Distortion Ratio (SI-SDR) and Mean Squared Error (MSE) as the evaluation metrics. Among these, MSE reflects the overall reconstruction accuracy of the separated signal relative to the reference signal. SDR measures the ratio of the target signal power to the energy of all distortion components (including noise, interference, and artifacts), serving as a comprehensive indicator of separation quality. SIR evaluates the suppression of interference from other sources in the target signal, while SAR quantifies the degree of artifacts introduced during the separation process, representing the proportion of artifacts in the separated signal. SI-SDR, as a scale-invariant extension of SDR, normalizes by gain to eliminate amplitude effects, providing a more robust measure of signal quality. In few-shot tasks, we further introduce the Kappa coefficient to assess the consistency of classification results and eliminate the influence of chance, serving as a more stringent metric for group classification consistency. These diverse evaluation metrics collectively provide a comprehensive quantitative foundation for evaluating the model's performance across multiple tasks and multi-dimensional scenarios.

*1) Classification:* In the classification task, the general feature representations extracted from the pretrained base model are fed into a linear classifier for category prediction, with cross-entropy adopted as the loss function. We evaluate performance across multiple datasets, including the communication modulation recognition datasets RML2016.10A [34], RML2016.10B [34], RML2016.04C [35], and RML2018.01A [15]; the emit-

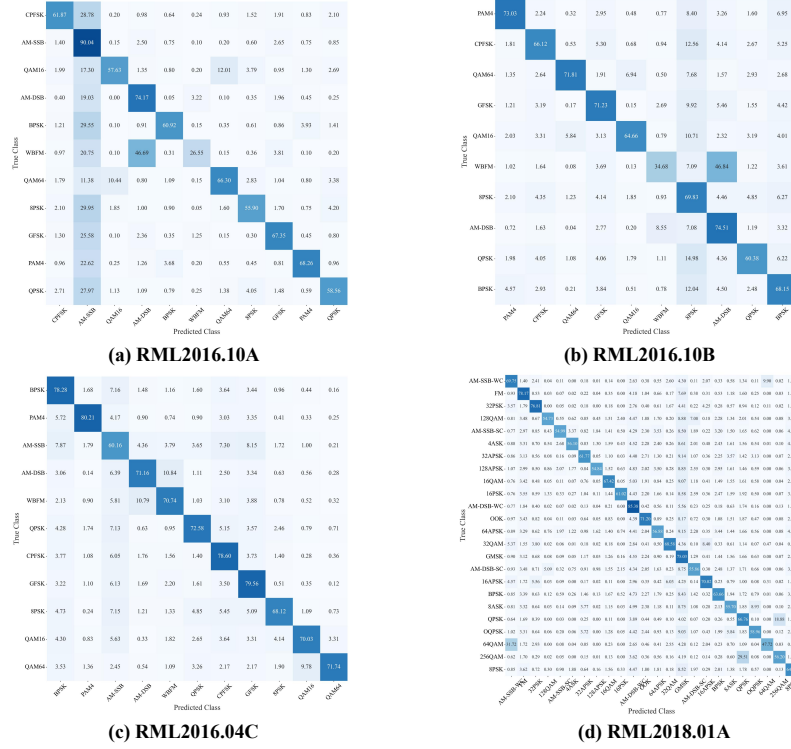


Fig. 8: Confusion matrices for EMind on different datasets. (a)-(d) show the confusion matrices for RML2016.10A, RML2016.10B, RML2016.04C, and RML2018.01A, respectively, highlighting the model's performance across various modulation categories.

ter identification datasets ADS-B [37] and EM-AIS; as well as the interference type recognition datasets EM-Infer-Comm and EM-Infer-Radar. Among them, EM-AIS is a proprietary dataset collected for shipborne emitter identification, while EM-Infer-Comm and EM-Infer-Radar are self-constructed synthetic datasets for interference classification. The signal lengths of these datasets are as follows: 128 for RML2016.10A, RML2016.10B, and RML2016.04C; 1,024 for RML2018.01A, EM-Infer-Comm, and EM-Infer-Radar; and 3,000 for ADS-B. Since the raw sequence length of EM-AIS is 11,520, to reduce computational overhead we perform threefold downsampling based on its bandwidth characteristics and the Nyquist sampling criterion, yielding a final signal length of 3,840. For dataset partitioning, we use 80% of the data for fine-tuning on RML2016.10A, RML2016.10B, RML2016.04C, and RML2018.01A; a 1:9 training-to-testing split for ADS-B, EM-Infer-Comm, and EM-Infer-Radar; and a 5:5 split for EM-AIS, as its limited data volume and large number of categories necessitate ensuring coverage of all classes in the training set.

*a) Automatic Modulation Classification and Radio Frequency Fingerprint Identification:* The classification experiment results are shown in Table V, where RML2016.10A [34], RML2016.10B [34], and RML2016.04C [35] use the contrastive algorithm setup from SpectrumFM [14]; while the comparison algorithms for the RML2018.01A [15], ADS-B [37], EM-Infer-Comm, EM-Infer-Radar and EM-AIS datasets are reproduced

based on the ResNet [38] and Transformer [20] models. The experimental results demonstrate that our model achieves state-of-the-art performance across Automatic Modulation Classification (AMC), Radio Frequency Fingerprint Identification (RFFI), and Wireless Interference Identification (WII) tasks. In AMC, EMind attains accuracies of 65.45% and 74.34% on RML2016.10B and RML2016.04C, respectively, surpassing all competing approaches, with a 0.97 percentage point improvement over SpectrumFM [14] on RML2016.04C. In RFFI, EMind achieves 99.87% accuracy on the ADS-B dataset, and further delivers 57.07% on the more challenging EM-AIS dataset, substantially outperforming the Transformer baseline (39.12%) and verifying the robustness of the proposed method under complex environments. For WII, EMind obtains 81.70% and 79.19% accuracy on EM-Infer-Comm and EM-Infer-Radar, respectively, outperforming all existing methods and further demonstrating the superior capability of our model in highly challenging signal recognition scenarios.

Figure 7 and Figure 8 present performance analysis at different signal-to-noise (SNR) ratios and confusion matrices for multiple communication datasets. Figure 7 compares the overall accuracy (OA) of EMind with other models under various SNR conditions; Figure 8 shows the confusion matrix for EMind, providing a detailed view of its classification performance across various modulation categories, highlighting both strengths and potential misclassification areas.

b) *Feature-based Approach*: To verify whether the pre-trained model has learned task-agnostic general representations, modulation classification experiments are conducted using a linear probing strategy in addition to full fine-tuning. In this setting, all pre-trained weights are frozen, and only a linear classifier appended to the output features is trained. This strategy minimizes the extent of parameter updates and is used to assess the linear separability and cross-task generalizability of the features, thereby providing a purer measure of the quality of the pre-trained representations. Compared to full fine-tuning, linear probing incurs lower computational overhead and directly reflects the inherent transferability of the pre-trained features.

As shown in Figure 9, we evaluate our model on four public datasets including RML2016.10A [34], RML2016.10B [34], RML2016.04C [35], and RML2018.01A [15], under three experimental settings: training from scratch, full fine-tuning, and linear probing. The results show that comparable accuracy to full fine-tuning is achieved by training only a single linear classifier on top of the frozen pre-trained features, demonstrating the generality and transferability of the learned representations. Furthermore, as illustrated in Figure 10, linear probing is performed on checkpoints from different pre-training epochs. It is observed that classification performance improves rapidly with increased pre-training duration and saturates at an early stage. This phenomenon indicates that the model acquires high-quality, linearly separable, and generalizable features early in training. Even when early-stage weights are used as fixed feature extractors, convergence of downstream tasks is significantly accelerated and final performance is enhanced.

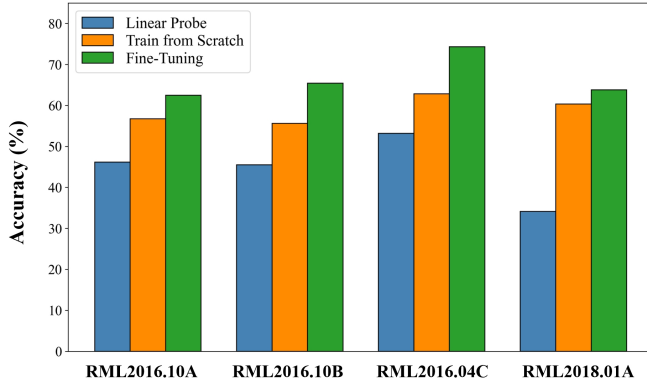


Fig. 9: Classification accuracy on four public datasets RML2016.10A, RML2016.10B, RML2016.04C, and RML2018.01A under three training strategies: training from scratch, linear probing, and full fine-tuning.

2) *Radar parameters estimation tasks*: For the regression task, the regression head outputs continuous values and is optimized using regression loss functions such as mean absolute error (MAE). In this task, multi-task joint regression is implemented by extending the regression head into a multi-output structure to support joint modeling of

multiple continuous variables, which is trained jointly with the classification task. The experiments are evaluated on the radar dataset RadChar [36], where radar waveform classification is performed, and four parameters—pulse number ( $n_p$ ), pulse width ( $t_{pw}$ ), pulse repetition interval ( $t_{pri}$ ), and pulse time delay ( $t_d$ )—are regressed. Specifically, the pulse number ranges from 2 to 6, pulse width ranges from 10 to 16  $\mu$ s, pulse repetition interval (PRI) ranges from 17 to 23  $\mu$ s, and pulse time delay ranges from 1 to 10  $\mu$ s. To ensure a fair comparison, the dataset split is set as 70:15:15, following [36], with a signal length of 512. The results are shown in Table VI, where classification accuracy is measured using overall accuracy (OA) and regression performance is measured using MAE. We test the performance on the test set at SNR of -10 dB, 0 dB, and 10 dB respectively, and also evaluate performance across all SNR range from -20 dB to 20 dB. Our joint classification-regression performance substantially outperforms the state-of-the-art (SOTA) methods.

3) *Blind source separation and Signal Denoise*: Blind Source Separation (BSS) is a highly challenging inverse problem in complex electromagnetic environments. Its goal is to recover the original, mutually independent source signals from observed mixed signals without prior knowledge of the source signal characteristics or the mixing process. Since only noisy IQ signals can be observed, which are from the mixing of an unknown number of radiation sources through unknown channels, the true number of sources cannot be known in advance, and no clean ground truth source signals are available during training. This problem is ill-posed, without additional assumptions a unique solution may not exist, and the system is highly sensitive to small perturbations in the input, especially in noisy IQ signal environments. Autoencoders are widely used in blind source separation tasks due to their ability to learn compact and discriminative latent representations from mixed signals. By mapping the mixed signals to a lower-dimensional latent space, autoencoders can separate the latent source signals in an unsupervised manner. To address the source separation task, a fine-tuning framework based on the Autoencoder (AE) architecture is implemented. A multi-layer linear compression layer is introduced on top of the pretrained model, and by constraining the decoder capacity, the model is forced to extract compact and discriminative latent features from the complex mixed signals. Specifically, as shown in Table VII, the linear compression layers are applied progressively according to predefined hidden dimensions, and the features are ultimately compressed and projected to a fixed number of  $K$  channels (with  $K = 2$  in our setting) through the final linear mapping, where each channel is represented by a 16-dimensional vector, reducing the complexity of signal representation. The core loss function consists of two components: the first is the reconstruction error loss, which supports the reconstruction of either the entire mixed signal or the separated independent signal channels. The latter addresses the signal order uncertainty using a permutation invariant training strategy, ensuring a high alignment between the training objective and the actual separation performance. The second component

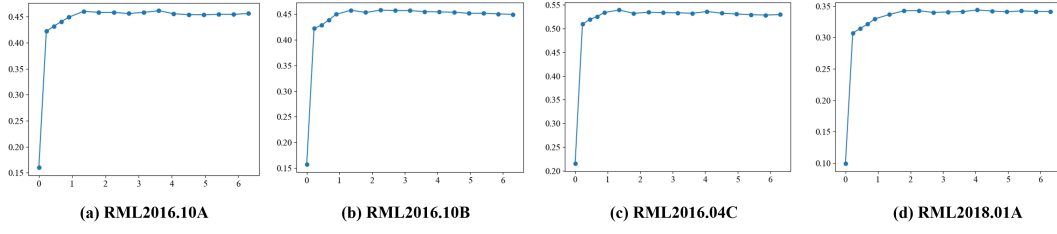


Fig. 10: Evaluation of linear probing accuracy on checkpoints from different pre-training epochs. Rapid saturation of performance indicates that transferable and linearly separable features are learned early during pre-training.

TABLE VI: Multi-task of RWC and RPE on RadChar [36]. BOLD indicates the best performance. Lower MAE indicates better regression performance, while higher accuracy reflects better classification.

Methods	MAE $n_p$ ( $\mu$ s)	MAE $t_{pw}$ ( $\mu$ s)	MAE $t_{pri}$ ( $\mu$ s)	MAE $t_d$ ( $\mu$ s)	Class Accuracy (%)
	-10db 0db 10db all <sup>†</sup>	-10db 0db 10db all	-10db 0db 10db all	-10db 0db 10db all	-10db 0db 10db all
CNN1D	0.729, 0.193, 0.085 -	1.413, 0.560, 0.340 -	0.999, 0.330, 0.209 -	1.349, 0.385, 0.206 -	75.7, 99.8, 100 -
CNN2D	0.793, 0.174, 0.090 -	1.466, 0.801, 0.505 -	1.054, 0.420, 0.299 -	1.729, 0.638, 0.443 -	67.3, 98.3, 99.8 -
IQST-S	0.733, 0.294, 0.251 -	1.282, 0.628, 0.364 -	0.816, 0.273, 0.192 -	1.229, 0.415, 0.277 -	79.2, 99.9, 100 -
IQST-L	0.752, 0.195, 0.124 -	1.253, 0.579, 0.334 -	0.799, 0.286, 0.225 -	1.253, 0.379, 0.233 -	79.1, 99.8, 100 -
<b>EMind</b>	<b>0.330, 0.006, 0.005, 0.114</b>	<b>0.797, 0.197, 0.080, 0.305</b>	<b>0.463, 0.109, 0.085, 0.221</b>	<b>0.708, 0.149, 0.092, 0.323</b>	<b>86.65, 100, 100, 88.49</b>

<sup>†</sup> all indicates that the results are evaluated across the entire SNR range from -20 dB to 20 dB.



Fig. 11: The BSS Eval comprises Signal-to-Distortion Ratio (SDR), Signal-to-Interference Ratio (SIR), Signal-to-Artifacts Ratio (SAR), Scale-Invariant Signal-to-Distortion Ratio (SI-SDR), and Mean Squared Error (MSE), where higher values of the first four indicate superior separation quality, whereas lower MSE signifies higher fidelity.

is the  $\ell_2$ -norm regularization term applied to the latent representations, which encourages the encoded features to remain stable, sparse, and discriminative, thus improving the generalization and robustness of the representation. This joint loss design not only optimizes the reconstruction accuracy of the signal but also promotes the model to learn stable and discriminative latent representations.

TABLE VII: Model layers architecture for the downstream task of blind source separation. Note:  $K = 2$ .

INPUT	Layer 1	Layer 2	Layer 3	Layer 4	OUTPUT
$D_{Enc} \times num_{patch}$	4096	2048	1536	1024	16K

TABLE VIII: Performance Comparison of Blind Source Separation (BSS) on EM-Radar-Mix.

Setting	SDR	SIR	SAR	SI-SDR	MSE
Linear prob	4.85	10.73	6.92	-5.88	-13.85
Fine-tune	5.74	11.60	7.83	-3.85	-15.32

The blind source separation task is evaluated on the self-constructed EM-Radar-Mix dataset. Due to the complexity and innovation of this task, there is currently a lack of suitable publicly available datasets, prompting the construction of this challenging dataset. The EM-Radar-Mix dataset consists of 123,200 samples, with 100,800 samples for the training set, 11,200 samples for the validation set, and 11,200 samples for the test set. The signal length is 1,024. The dataset contains 8 types of original radar signals, which are mixed under conditions of a 5 MHz sampling rate and a signal-to-noise ratio (SNR) set to 12 dB. During sample construction, these signals are mixed either in pairs or individually, and the specific signal types mixed in each sample are unknown to the model, thereby creating a typical blind source separation task scenario.

A series of standardized evaluation metrics defined in the BSS Eval toolkit [45] are used to assess the performance of 100 randomly sampled signal samples from the test set. The selected evaluation metrics include Signal-to-Distortion Ratio (SDR), Signal-to-Interference Ratio (SIR), Signal-to-Artifacts Ratio (SAR), Scale-Invariant Signal-to-Distortion Ratio (SI-SDR), and Mean Squared Error (MSE). These

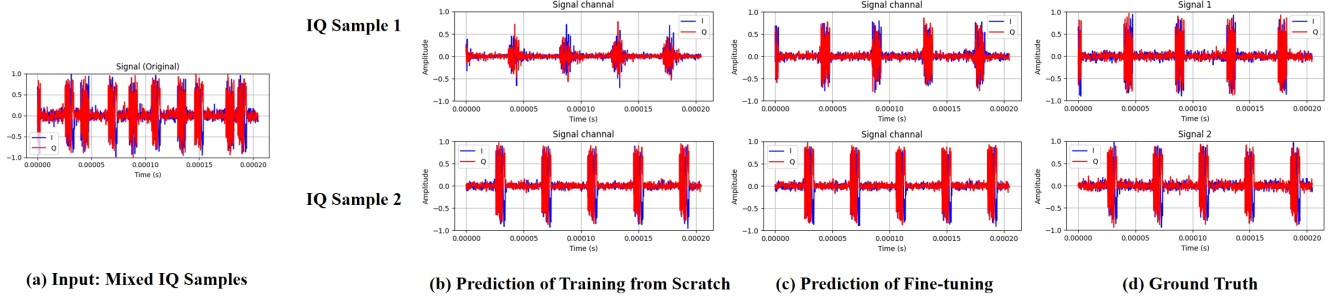


Fig. 12: Visualization of IQ signal blind source separation (BSS) results. (a) mixed IQ signal input, (b) separation results of training from scratch, (c) separation results with fine-tuning, (d) ground truth.

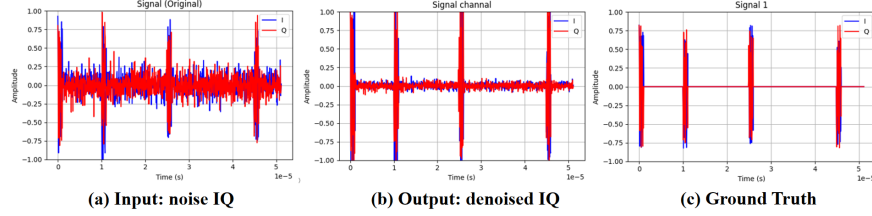


Fig. 13: Visualization of IQ signal denoising. (a) noisy IQ input. (b) denoised prediction. (c) ground truth. The comparison illustrates the model’s effectiveness in removing noise, achieving excellent consistency in amplitude and phase alignment.

TABLE IX: Comparison of Methods for few shot on classification tasks. BOLD indicates the best performance.

TASK	AMC				RWC					
	RML2016.10A				RadChar					
	50 shot		100 shot		10 shot		50 shot		100 shot	
METHOD	OA(%)	Kappa	OA(%)	Kappa	OA(%)	Kappa	OA(%)	Kappa	OA(%)	Kappa
ResNet	38.97	32.87	42.01	36.21	71.94	64.93	79.89	74.86	80.97	76.21
Transformer	38.40	32.25	39.81	33.79	64.27	55.37	76.42	70.52	79.21	74.01
EMind	<b>48.38</b>	<b>42.85</b>	<b>50.10</b>	<b>45.12</b>	<b>78.37</b>	<b>72.97</b>	<b>81.94</b>	<b>77.43</b>	<b>83.14</b>	<b>78.93</b>

metrics are widely recognized performance measures in the Blind Source Separation (BSS) field, providing a comprehensive reflection of the model’s distortion level, interference suppression effectiveness, and separation accuracy during signal reconstruction.

Through the analysis of the quantitative assessment results (Table VIII) and the comparative curves (Figure 11), we conducted an in-depth comparison between the Linear Probe (LP) and Fine-tune (FT) strategies. The Fine-tune strategy, which optimizes all model parameters, achieves superior performance under adequate training conditions. The comparative curves presented in Figure 11 further reveal the advantages of pre-trained weights and the performance of both strategies in terms of feature learning ability. The FT strategy’s curves rise rapidly at the beginning of training, demonstrating its characteristic of fast convergence, indicating that pre-trained weights facilitate the model in quickly learning and achieving better performance. Although the LP strategy has a slower initial rise in the curves, their gradual ascent during the training process shows that the LP strategy can effectively extract general features from the pre-

trained model and improve signal separation performance to a certain extent. Integrating the analysis of Table VIII and Figure 11, we can conclude that pre-trained models exhibit exceptional feature learning capabilities when performing generative reconstruction tasks, especially under the Fine-tune scenario. The FT strategy not only converges quickly but also shows higher values in all evaluation metrics, except for the Mean Squared Error (MSE), where a lower value indicates better performance. These results not only validate the effectiveness of the proposed unsupervised generative reconstruction fine-tuning framework but also highlight the potential and advantages of pre-trained models in signal separation tasks.

Figure 12 shows the visualization results of the blind source separation task. Figure 12 (a) is the input mixed IQ signals, Figure 12 (b) shows the separation results from training from scratch, Figure 12 (c) shows the separation results after fine-tuning by loading the pre-trained model, and (d) is the ground truth. From these visualizations, we can intuitively observe the profound impact of pre-trained model on performance. After loading the pre-trained model,

the model quickly converges to the ideal separation results, successfully distinguishing signals from different sources, and performing excellently in terms of signal integrity and accuracy. In contrast, without pre-trained weights, the solution to this ill-posed problem tends to be infinitely many, and unsupervised training struggles to obtain a sufficiently general representation of IQ signals. The model faces significant difficulties in signal separation, unable to effectively extract the key features of the signals, ultimately leading to separation failure.

Furthermore, we introduce our self-built EM-Denoise-Signal dataset within this framework to conduct denoising experiments on IQ signals. The dataset simulates various interference factors in real-world environments, including Gaussian white noise (AWGN) ranging from -3 dB to 20 dB, along with common hardware impairments such as system frequency offset ( $\pm 50$  kHz), IQ amplitude imbalance, and phase imbalance. For our model framework, the input consists of noisy signals, with no denoised signals available as supervision. Using an autoencoder, the model is able to separate the true signal from the noisy input. Figure 13 presents the model's visualization results for this task. As shown in the figure, under the noisy input in Figure 13 (a), the denoised result in Figure 13 (b) is compared with the Ground Truth in Figure 13 (c). The comparison reveals excellent consistency in amplitude alignment and phase restoration, demonstrating the model's capability to accurately model and recover the signal structure in complex interference environments.

4) *Few-shot*: The few-shot classification experiments were conducted on two datasets: RML2016.10A for modulation classification and RadChar for radar waveform classification. For RML2016.10A, we followed a standard few-shot learning paradigm by randomly selecting 50 or 100 samples per modulation class and SNR level from the training set to form the support set, while the remaining samples were used for validation and testing. Similarly, for RadChar, experiments were performed under 10-shot, 50-shot, and 100-shot settings, with the support set exclusively drawn from the training data. To ensure a fair and challenging evaluation, the testing phase strictly used unseen signals, assessing the model's generalization capability in real-world scenarios. As shown in Table IX, our proposed EMind method achieves the best performance across all few-shot settings. On RML2016.10A, EMind attains an OA of 48.38% (Kappa: 42.85%) in the 50-shot case and further improves to 50.10% (Kappa: 45.12%) in the 100-shot case, outperforming ResNet and Transformer baselines. For RadChar, EMind demonstrates strong few-shot learning ability, achieving OAs of 78.37%, 81.94%, and 83.14% under 10-shot, 50-shot, and 100-shot conditions, respectively, with corresponding Kappa coefficients of 72.97%, 77.43%, and 78.93%. These results validate the robustness and generalization capability of EMind in EM signal classification, particularly in data-scarce scenarios.

## VII. CONCLUSION

The proposed EMind model not only provides a high-performance foundation that can be directly fine-tuned for various electromagnetic tasks, but more importantly, as an EM signals foundation model, it generates general representations with high transferability. In the upcoming era of multimodal large models, these representations can be compared to visual encoders in visual large models, transforming complex and heterogeneous EM signals into compact, semantically rich feature vectors. This provides a unified interface for subsequent integration into larger-scale cross-modal models. Experiments show that the features extracted by EMind maintain excellent performance even without fine-tuning, further proving that the next stage of electromagnetic intelligence is no longer about training a small model for each task, but rather using EMind to extract features once that can be shared across countless downstream large models.

## REFERENCES

- [1] Xiaoyang Hao, Zhixi Feng, Ruoyu Liu, Shuyuan Yang, Licheng Jiao, and Rong Luo. Contrastive self-supervised clustering for specific emitter identification. *IEEE Internet of Things Journal*, 10(23):20803–20818, 2023.
- [2] Zhengming Zhang, Taotao Ji, Haoqing Shi, Chunguo Li, Yongming Huang, and Luxi Yang. A self-supervised learning-based channel estimation for irs-aided communication without ground truth. *IEEE Transactions on Wireless Communications*, 22(8):5446–5460, 2023.
- [3] Longlong Jing and Yingli Tian. Self-supervised visual feature learning with deep neural networks: A survey. *IEEE transactions on pattern analysis and machine intelligence*, 43(11):4037–4058, 2020.
- [4] Ce Zhou, Qian Li, Chen Li, Jun Yu, Yixin Liu, Guangjing Wang, Kai Zhang, Cheng Ji, Qiben Yan, Lifang He, et al. A comprehensive survey on pretrained foundation models: A history from bert to chatgpt. *International Journal of Machine Learning and Cybernetics*, pages 1–65, 2024.
- [5] Jaron Fontaine, Adnan Shahid, and Eli De Poorter. Towards a wireless physical-layer foundation model: Challenges and strategies. In *2024 IEEE International Conference on Communications Workshops (ICC Workshops)*, pages 1–7. IEEE, 2024.
- [6] Yucheng Sheng, Jiacheng Wang, Xingyu Zhou, Le Liang, Hao Ye, Shi Jin, and Geoffrey Ye Li. A wireless foundation model for multi-task prediction. *arXiv preprint arXiv:2507.05938*, 2025.
- [7] Yuxuan Liang, Haomin Wen, Yuqi Nie, Yushan Jiang, Ming Jin, Dongjin Song, Shirui Pan, and Qingsong Wen. Foundation models for time series analysis: A tutorial and survey. In *Proceedings of the 30th ACM SIGKDD conference on knowledge discovery and data mining*, pages 6555–6565, 2024.
- [8] Chaoyun Zhang, Paul Patras, and Hamed Haddadi. Deep learning in mobile and wireless networking: A survey. *IEEE Communications surveys & tutorials*, 21(3):2224–2287, 2019.
- [9] Berkay Guler, Giovanni Geraci, and Hamid Jafarkhani. A multi-task foundation model for wireless channel representation using contrastive and masked autoencoder learning. *arXiv preprint arXiv:2505.09160*, 2025.
- [10] Tingting Yang, Ping Zhang, Mengfan Zheng, Yuxuan Shi, Liwen Jing, Jianbo Huang, and Nan Li. Wirelessgpt: A generative pre-trained multi-task learning framework for wireless communication. *IEEE Network*, 2025.
- [11] Jakob Hoydis, Sebastian Cammerer, Fayçal Ait Aoudia, Avinash Vem, Nikolaus Binder, Guillermo Marcus, and Alexander Keller. Sionna: An open-source library for next-generation physical layer research. *arXiv preprint arXiv:2203.11854*, 2022.
- [12] Ahmed Alkhateeb. Deepmimo: A generic deep learning dataset for millimeter wave and massive mimo applications. *arXiv preprint arXiv:1902.06435*, 2019.
- [13] Ahmed Aboufotouh, Elsayed Mohammed, and Hatem Abou-Zeid. 6g wavesfm: A foundation model for sensing, communication, and localization. *arXiv preprint arXiv:2504.14100*, 2025.

- [14] Fuhui Zhou, Chunyu Liu, Hao Zhang, Wei Wu, Qihui Wu, Derrick Wing Kwan Ng, Tony QS Quek, and Chan-Byoung Chae. Spectrumfm: A foundation model for intelligent spectrum management. *arXiv preprint arXiv:2505.06256*, 2025.
- [15] Timothy James O'Shea, Tamoghna Roy, and T Charles Clancy. Over-the-air deep learning based radio signal classification. *IEEE Journal of Selected Topics in Signal Processing*, 12(1):168–179, 2018.
- [16] Jaron Fontaine, Erika Fonseca, Adnan Shahid, Maicon Kist, Luiz A DaSilva, Ingrid Moerman, and Eli De Poorter. Towards low-complexity wireless technology classification across multiple environments. *Ad Hoc Networks*, 91:101881, 2019.
- [17] Muhammad Awais, Muzammal Naseer, Salman Khan, Rao Muhammad Anwer, Hisham Cholakkal, Mubarak Shah, Ming-Hsuan Yang, and Fahad Shahbaz Khan. Foundation models defining a new era in vision: a survey and outlook. *IEEE Transactions on Pattern Analysis and Machine Intelligence*, 2025.
- [18] Yu Han, Xiaofeng Liu, Xiang Zhang, and Cheng Ding. Foundation models in electrocardiogram: A review. *arXiv preprint arXiv:2410.19877*, 2024.
- [19] Danfeng Hong, Bing Zhang, Xuyang Li, Yuxuan Li, Chenyu Li, Jing Yao, Naoto Yokoya, Hao Li, Pedram Ghamisi, Xiuping Jia, et al. Spectralgpt: Spectral remote sensing foundation model. *arXiv preprint arXiv:2311.07113*, 2023.
- [20] Ashish Vaswani, Noam Shazeer, Niki Parmar, Jakob Uszkoreit, Llion Jones, Aidan N Gomez, Łukasz Kaiser, and Illia Polosukhin. Attention is all you need. *Advances in neural information processing systems*, 30, 2017.
- [21] K Tekbiyik, C Keçeci, AR Ekti, A Görçin, and G Kurt. Hisarmod: A new challenging modulated signals dataset. *IEEE Dataport*, 2019.
- [22] Stefan Scholl. Classification of radio signals and hf transmission modes with deep learning. *arXiv preprint arXiv:1906.04459*, 2019.
- [23] Anu Jagannath and Jithin Jagannath. Dataset for modulation classification and signal type classification for multi-task and single task learning. *Computer Networks*, 199:108441, 2021.
- [24] Samer Hanna, Samurdhi Karunaratne, and Danijela Cabric. Wisig: A large-scale wifi signal dataset for receiver and channel agnostic rf fingerprinting. *IEEE Access*, 10:22808–22818, 2022.
- [25] Amani Al-Shawabka, Francesco Restuccia, Salvatore D'Oro, Tong Jian, Bruno Costa Rendon, Nasim Soltani, Jennifer Dy, Stratis Ioannidis, Kaushik Chowdhury, and Tommaso Melodia. Exposing the fingerprint: Dissecting the impact of the wireless channel on radio fingerprinting. In *IEEE INFOCOM 2020-IEEE Conference on Computer Communications*, pages 646–655. IEEE, 2020.
- [26] Guillem Reus-Muns, Dheryta Jaisinghani, Kunal Sankhe, and Kaushik R Chowdhury. Trust in 5g open rans through machine learning: Rf fingerprinting on the powder pawr platform. In *GLOBECOM 2020-2020 IEEE Global Communications Conference*, pages 1–6. IEEE, 2020.
- [27] Cyrille Morin, Leonardo S Cardoso, Jakob Hoydis, Jean-Marie Gorce, and Thibaud Vial. Transmitter classification with supervised deep learning. In *International Conference on Cognitive Radio Oriented Wireless Networks*, pages 73–86. Springer, 2019.
- [28] Abdurrahman Elmaghbbub and Bechir Hamdaoui. Lora device fingerprinting in the wild: Disclosing rf data-driven fingerprint sensitivity to deployment variability. *IEEE Access*, 9:142893–142909, 2021.
- [29] Yongxin Liu, Jian Wang, Jianqiang Li, Houbing Song, Thomas Yang, Shuteng Niu, and Zhong Ming. Zero-bias deep learning for accurate identification of internet-of-things (iot) devices. *IEEE Internet of Things Journal*, 8(4):2627–2634, 2020.
- [30] Ningning Yu, Shengjian Mao, Chengwei Zhou, Guowei Sun, Zhiguo Shi, and Jiming Chen. Dronerfa: A large-scale dataset of drone radio frequency signals for detecting low-altitude drones. *Journal of Electronics & Information Technology*, 46(4):1147–1156, 2024.
- [31] Guoxuan Chi, Zheng Yang, Chenshu Wu, Jingao Xu, Yuchong Gao, Yunhao Liu, and Tony Xiao Han. Rf-diffusion: Radio signal generation via time-frequency diffusion. In *Proceedings of the 30th Annual International Conference on Mobile Computing and Networking*, pages 77–92, 2024.
- [32] Shuai Chen, Zhixi Feng, Shuyuan Yang, Yue Ma, Jun Liu, and Zhuoyue Qi. A generative self-supervised framework for cognitive radio leveraging time-frequency features and attention-based fusion. *IEEE Transactions on Wireless Communications*, 2024.
- [33] Shuai Chen, Yong Zu, Zhixi Feng, Shuyuan Yang, and Mengchang Li. Radiollm: Introducing large language model into cognitive radio via hybrid prompt and token reprogrammings. *arXiv preprint arXiv:2501.17888*, 2025.
- [34] Timothy J O'shea and Nathan West. Radio machine learning dataset generation with gnu radio. In *Proceedings of the GNU radio conference*, volume 1, 2016.
- [35] Timothy J O'Shea, Johnathan Corgan, and T Charles Clancy. Convolutional radio modulation recognition networks. In *International conference on engineering applications of neural networks*, pages 213–226. Springer, 2016.
- [36] Zi Huang, Akila Pemasiri, Simon Denman, Clinton Fookes, and Terrence Martin. Multi-task learning for radar signal characterisation. In *2023 IEEE International Conference on Acoustics, Speech, and Signal Processing Workshops (ICASSPW)*, pages 1–5. IEEE, 2023.
- [37] TU Ya, LIN Yun, ZHA Haoran, WANG Yu, GUI Guan, MAO Shiwen, et al. Large-scale real-world radio signal recognition with deep learning. *Chinese Journal of Aeronautics*, 35(9):35–48, 2022.
- [38] Kaiming He, Xiangyu Zhang, Shaoqing Ren, and Jian Sun. Deep residual learning for image recognition. In *Proceedings of the IEEE conference on computer vision and pattern recognition*, pages 770–778, 2016.
- [39] Thien Huynh-The, Cam-Hao Hua, Quoc-Viet Pham, and Dong-Seong Kim. Mcnet: An efficient cnn architecture for robust automatic modulation classification. *IEEE Communications Letters*, 24(4):811–815, 2020.
- [40] Dehua Hong, Zilong Zhang, and Xiaodong Xu. Automatic modulation classification using recurrent neural networks. In *2017 3rd IEEE international conference on computer and communications (ICCC)*, pages 695–700. IEEE, 2017.
- [41] Ziqi Ke and Haris Vikalo. Real-time radio technology and modulation classification via an lstm auto-encoder. *IEEE Transactions on Wireless Communications*, 21(1):370–382, 2021.
- [42] Judith Nkechinyere Njoku, Manuel Eugenio Morocho-Cayamcela, and Wansu Lim. Cgdnet: Efficient hybrid deep learning model for robust automatic modulation recognition. *IEEE Networking Letters*, 3(2):47–51, 2021.
- [43] Hao Zhang, Fuhui Zhou, Qihui Wu, Wei Wu, and Rose Qingyang Hu. A novel automatic modulation classification scheme based on multi-scale networks. *IEEE Transactions on Cognitive Communications and Networking*, 8(1):97–110, 2021.
- [44] Jiawei Zhang, Tiantian Wang, Zhixi Feng, and Shuyuan Yang. Amcnet: An effective network for automatic modulation classification. In *ICASSP 2023-2023 IEEE International Conference on Acoustics, Speech and Signal Processing (ICASSP)*, pages 1–5. IEEE, 2023.
- [45] Emmanuel Vincent, Rémi Gribonval, and Cédric Févotte. Performance measurement in blind audio source separation. *IEEE transactions on audio, speech, and language processing*, 14(4):1462–1469, 2006.